



Design and Dynamic Performance Analysis of High-Contact-Ratio Spiral Bevel Gear Based on Ease-off Technology

Yan-Ming Mu^{1,2} · Xue-Ming He^{1,2} · Zong-De Fang³

Received: 12 August 2020 / Revised: 27 June 2021 / Accepted: 29 August 2021 / Published online: 28 October 2021
© Korean Society for Precision Engineering 2021

Abstract

To improve the dynamic performance of spiral bevel gear transmission, an ease-off flank modification method of the high-contact-ratio spiral bevel gear is proposed. First, the high-contact-ratio spiral bevel gear is designed by increasing the angle between the contact path and the pitch cone of a pinion tooth surface with ease-off technology. Second, the meshing performance of the high-contact-ratio spiral bevel gear designed utilizing ease-off technology is compared with the HCR spiral bevel gear designed by the local synthesis method. Finally, the loaded transmission error (the main vibration excitation of the gear transmission in the low-speed range), the meshing impact (the main vibration excitation of the gear transmission in the high-speed range) and the dynamic performance of the high-contact-ratio spiral bevel gear are compared with that of a low-contact-ratio spiral bevel gear. A simulation analysis based on the ease-off technology shows that the design contact ratio of the spiral bevel gear can be improved by increasing the angle between the contact path and the pitch cone of the pinion tooth surface; compared with the local synthesis method, the high-contact-ratio spiral bevel gear transmission designed by the ease-off flank modification method has a better meshing performance; increasing the design contact ratio can effectively reduce the loaded transmission error, and meshing impact, and obtain a spiral bevel gear transmission with good dynamic performance over the whole speed range.

Keywords Spiral bevel gear · Ease-off · Design contact ratio · Dynamic performance · Load transmission errors · Meshing impact

1 Introduction

The power transmission system is an important part of the helicopter power system. Spiral bevel gears are widely used in helicopter power transmission systems because of their advantages. In recent years, helicopter engine performance has improved with improvements in science and technology,

and helicopter's power has also increased. Unfortunately, the running vibration of the spiral bevel gear also increases with the increasing helicopter power. Spiral bevel gears have high strength and dynamic performance requirements. The contact path of the traditional spiral bevel gear is approximately perpendicular to the root cone [1], and its *design contact ratio* (DCR) and strength are both low. How to increase the DCR and improve the strength performance of spiral bevel gears has attracted extensive attention from experts [2]. Based on the *local synthesis method* (LSM), Deng improved the DCR of the spiral bevel gear, and he also analyzed the strength performance of the HCR spiral bevel gear [3–7].

In view of the defects of Gleason Technology based on Literatures [8, 9], Litvin [10, 11] proposed the LSM. However, the LSM cannot control the meshing characteristics of the tooth surface far away from the reference point. Therefore, Oricon developed ease-off technology, which has been subject to much research by experts. Shih [12–14] provided a detailed definition of ease-off technology, proposed the tooth surface design method for the spiral bevel gear based on

✉ Yan-Ming Mu
muyanmingbest@163.com

Xue-Ming He
604756697@qq.com

¹ Jiangsu Key Laboratory of Advanced Food Manufacturing Equipment and Technology, Jiangnan University, Wuxi 214-122, People's Republic of China

² School of Mechanical Engineering, Jiangnan University, Wuxi 214-122, People's Republic of China

³ School of Mechanical Engineering, Northwestern Polytechnical University, Xi'an 710-072, People's Republic of China

ease-off technology, and finally verified it through computer simulation. Based on the ease-off technology, Stadtfeld [15] modified the pinion tooth surface of the spiral bevel gear, Kolivand [16, 17] studied the loaded meshing performance of the spiral bevel gear, and proposed the best ease-off tooth surface to reduce the LTE and contact stress of the hypoid gears. Artoni [18, 19] established a least square model of the hypoid gear based on the ease-off technology to optimize the *loaded transmission error* (LTE) and obtained the corresponding machining parameters. Fan [20] analyzed the ease-off theory and its application in the contact analysis of the spiral bevel gears and hypoid gears in detail. To improve the meshing performance of the spiral bevel gear, Wang [21] proposed a tooth surface modification method based on ease-off technology. Ding [22–25] proposed the machine parameter identification algorithm for the hypoid gear based on nonlinear analysis and the multi-objective optimization method for the meshing performance of the spiral bevel gear based on nonlinear interval optimization algorithm to evaluate the tooth contact performance. Mu [26–29] presented a new method to design a high-order transmission error for the HCR spiral bevel gear by the modified curvature motion method to reduce or eliminate gear vibration based on ease-off.

Due to scientific advancement, the spiral bevel gears are developing towards obtaining high-speeds and heavy-loads, and the problem of spiral bevel gear running vibration is becoming increasingly prominent. The running vibration of the spiral bevel gear not only leads to the unstable operation of the transmission system; but also causes the failure of the transmission system. The running vibration of the spiral bevel gear has increasingly become a bottleneck problem affecting product quality. The dynamic performance analysis and control of spiral bevel gears have become a problem that must be solved in modern industry.

To improve the meshing performance of spiral bevel gears and improve the design level of helicopter power transmission system, a HCR design method for the spiral bevel gear is proposed based on ease-off technology, and its dynamic performance is analyzed. Through comparative analysis, it is verified that ease-off technology can overcome the contrast of HCR spiral bevel gears designed by the LSM. Combined with ease-off technology, the HCR spiral bevel gear is designed by improving the angle between the contact path and pitch cone of pinion tooth surface. Through comparative analysis, the advantages of HCR design in reducing the load transmission error and meshing impact of spiral bevel gear and improving the dynamic performance of spiral bevel gear are verified. The HCR design method based on ease-off technology can be used for the design and analysis of other gear pairs.

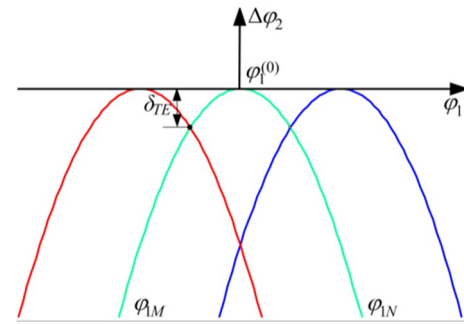


Fig. 1 Geometrical transmission error

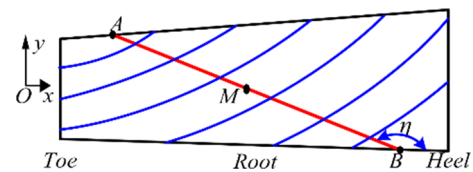


Fig. 2 The contact path

2 Design of DCR Spiral Bevel Gear Based on Ease-off

2.1 Geometric Transmission Error

The concave *transmission error* (TE) curve is shown in Fig. 1, where φ_1 is the pinion rotation angle, and δ is the TE amplitude. A detailed introduction to the TE curve is given in Literature 27.

The concave TE curve is defined as follows:

$$\begin{cases} \varphi_2 = \varphi_2^{(0)} + (\varphi_1 - \varphi_1^{(0)})Z_1/Z_2 \delta\varphi_2 \\ \delta\varphi_2 = -\delta_{TE}(\varphi_1 - \varphi_1^{(0)})^2 Z_1^2/\pi^2 \end{cases} \quad (1)$$

where $\varphi_2^{(0)}$ and $\varphi_1^{(0)}$ denote the original rotation angles, while Z_2 and Z_1 denote the tooth numbers.

2.2 Contact Path

The contact path of the spiral bevel gear runs through the whole working surface. The DCR of the spiral bevel gear is closely related to the contact path. When the contact path is perpendicular to the pitch cone, the DCR is smallest. Increasing the angle between the contact path and the pitch cone can increase the DCR. Based on the requirements of the DCR, the straight-line contact path on the pinion tooth surface shown in Fig. 2 is designed, and its equation is as follows:

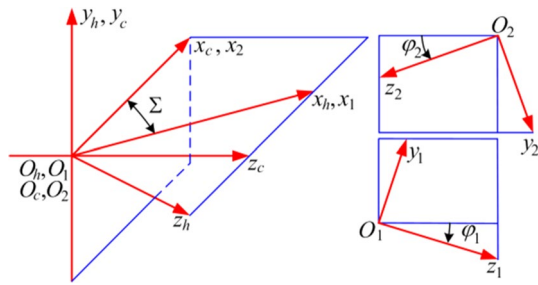


Fig. 3 The virtual gear cutter and pinion auxiliary surface

$$y = (x - x_M) \tan \eta + y_M \tag{2}$$

where (x_M, y_M) are the coordinates of the reference point M .

2.3 Pinion Auxiliary Tooth Surface

The gear tooth surface is treated as a virtual cutter to create pinion auxiliary surface based on the predesigned TE, as shown in Fig. 3. The coordinate systems S_1 and S_2 are rigidly attached to the pinion and the gear cutter, respectively.

The gear tooth surface is given by:

$$\begin{cases} r_2 = r_2(s_g, \theta_g, \varphi_g) \\ n_2 = n_2(s_g, \theta_g, \varphi_g) \\ f_2(s_g, \theta_g, \varphi_g) = 0 \end{cases} \tag{3}$$

where s_g and θ_g are the surface parameters, φ_g is the gear cradle angle, r_2 is the position vector of the gear tooth surface, n_2 is the unit normal vector of the gear tooth surface. f_2 denotes the meshing equation between the cutter and gear.

The parameters of the pinion auxiliary surface are calculated as follows:

$$\begin{cases} r'_1 = M_{1h}(\varphi_1)M_{h2}(\varphi_2)r_2 \\ n'_1 = L_{1h}(\varphi_1)L_{h2}(\varphi_2)n_2 \\ f_{12}(s_g, \theta_g, \varphi_g, \varphi_1) = 0 \end{cases} \tag{4}$$

where φ_1 is the pinion rotation angle, φ_2 is the gear cutter rotation angle, and f_{12} indicates the meshing equation between gear cutter and pinion. Matrices M_{h2} and M_{1h} are the homogenous coordinate transform matrices from S_2 to S_h and S_h to S_1 , respectively. L_{1h} and L_{h2} are the upper-left 3×3 sub-matrix of M_{1h} and M_{h2} , respectively.

$$M_{h2} = \begin{bmatrix} \cos \Sigma & \sin \Sigma \sin \phi_2 & -\sin \Sigma \cos \phi_2 & 0 \\ 0 & -\cos \phi_2 & -\sin \phi_2 & 0 \\ -\sin \Sigma & \cos \Sigma \sin \phi_2 & -\cos \Sigma \cos \phi_2 & 0 \\ 0 & 0 & 0 & 1 \end{bmatrix}$$

$$M_{1h} = \begin{bmatrix} 1 & 0 & 0 & 0 \\ 0 & \cos \varphi_1 & \sin \varphi_1 & 0 \\ 0 & -\sin \varphi_1 & \cos \varphi_1 & 0 \\ 0 & 0 & 0 & 1 \end{bmatrix}$$

2.4 Pinion Target Tooth Surface

To obtain the ease-off target surface, the pinion auxiliary surface needs to be modified along the instantaneous meshing line. The pinion auxiliary surface and the target surface are divided into q meshing points, and the position vector and unit normal vector of discrete point i ($i = 1, 2, \dots, q$) on the pinion auxiliary surface are presented as follows:

$$\begin{cases} p'_i = p'(s_g, \theta_g, \varphi_g, \phi_1) \\ n'_i = n'_i(s_g, \theta_g, \varphi_g, \phi_1) \end{cases} \tag{5}$$

where p' is the position vector of the discrete points, and n' is the unit normal vector of the discrete points.

The position vector of the discrete points on the target surface (shown in Fig. 4) can be obtained based on the following equation:

$$p_i^* = p'_i + n'_i \delta_{yi} \tag{6}$$

where δ_{yi} represent the flank modification value.

2.5 Calculation of Pinion Machining Parameters

The position vector r_p and the normal vector n_p of the pinion cutting cone are as follows:

$$r_p(s_p, \theta_p) = \begin{bmatrix} (R_p + s_p \sin \alpha_1) \cos \theta_p \\ (R_p + s_p \sin \alpha_1) \sin \theta_p \\ -s_p \cos \alpha_1 \\ 1 \end{bmatrix} \tag{7}$$

$$n_p(\theta_p) = \begin{bmatrix} \cos \alpha_1 \cos \theta_p \\ \cos \alpha_1 \sin \theta_p \\ -\sin \alpha_1 \end{bmatrix} \tag{8}$$

where s_p and θ_p are the cutter-head parameters, R_p is the cutter radius, and α_1 represents the profile angle.

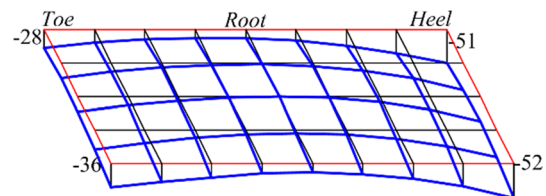


Fig. 4 Ease-off target tooth surface

The position vector r_1 of the pinion tooth surface is as follows:

$$r_1 = M_{1p}r_p \tag{9}$$

where

$$M_{1p} = \begin{bmatrix} a_{11} & a_{12} & a_{13} & a_{14} \\ a_{21} & a_{22} & a_{23} & a_{24} \\ a_{31} & a_{32} & a_{33} & a_{34} \\ a_{41} & a_{42} & a_{43} & a_{44} \end{bmatrix}$$

$$\begin{aligned} a_{11} &= \cos \gamma_1 \cos \phi_p \\ a_{12} &= -\cos \gamma_1 \sin \phi_p \\ a_{13} &= \sin \gamma_1 \\ a_{14} &= S_{r1} \cos \gamma_1 \cos \phi_p \cos q_1 - X_{b1} \sin \gamma_1 - X_{G1} - S_{r1} \cos \gamma_1 \sin \phi_p \sin q_1 \\ a_{21} &= \cos \phi_1 \sin \phi_p - \cos \phi_p \sin \gamma_1 \sin \phi_1 \\ a_{22} &= \cos \phi_1 \cos \phi_p + \sin \phi_p \sin \gamma_1 \sin \phi_1 \\ a_{23} &= \cos \gamma_1 \sin \phi_1 \\ a_{24} &= E_{m1} \cos \phi_1 - X_{b1} \cos \gamma_1 \sin \phi_1 + S_{r1} \sin q_1 (\cos \phi_1 \sin \phi_p - \cos \phi_p \sin \gamma_1 \sin \phi_1) \\ &\quad + S_{r1} \sin q_1 (\cos \phi_1 \cos \phi_p + \sin \gamma_1 \sin \phi_1 \sin \phi_p) \\ a_{31} &= -\sin \phi_1 \sin \phi_p - \cos \phi_p \sin \gamma_1 \cos \phi_1 \\ a_{32} &= -\cos \phi_1 \sin \gamma_1 \sin \phi_p - \cos \phi_p \sin \phi_1 \\ a_{33} &= \cos \gamma_1 \cos \phi_1 \\ a_{34} &= -E_{m1} \sin \phi_1 - X_{b1} \cos \gamma_1 \cos \phi_1 - S_{r1} \cos q_1 (\sin \phi_1 \sin \phi_p + \cos \phi_p \sin \gamma_1 \cos \phi_1) - S_{r1} \sin q_1 (\sin \phi_1 \cos \phi_p - \sin \gamma_1 \cos \phi_1 \sin \phi_p) \\ a_{41} &= a_{42} = a_{43} = 0 \cdot a_{44} = 1 \end{aligned}$$

Then the position vectors and the unit normal vectors of the discrete points on the pinion modification surface are as follows:

$$\begin{cases} p_i = r_1(s_{pi}, \theta_{pi}, \varphi_{pi}) \\ n_i = n_1(\theta_{pi}, \varphi_{pi}) \end{cases} \tag{10}$$

The deviation between the pinion modification surface and the target surface at the discrete points can be expressed by the following equations:

$$h_i = (p_i^* - p_i)n_i \tag{11}$$

$$h = [h_1, h_2, h_3, \dots, h_k]^T \tag{12}$$

Finally, the optimization model is established as shown in Eq. (13), in which the pinion machining parameters L are variables and the minimum sum of squares of the normal deviation between the pinion modification surface and the target surface is the object. In this paper, the NSGA-II algorithm is used, and the corresponding Matlab program is written to solve the optimization model:

$$\min f(L^{(i)}) = \frac{1}{2} h^T h \tag{13}$$

3 Calculation of Vibration Excitation

3.1 LTE

LTE is the main vibration excitation of the spiral bevel gear transmission in the low speed range, and it can be

obtained by the LTCA method [30]. Figure 5 shows the LTCA model of the spiral bevel gear, and the LTE can be obtained by transforming the normal displacement Z into angular displacement.

Before load is applied to the gear, the initial clearance between two meshing teeth is as follows:

$$w_k = \delta_k'' + b_k \quad k = I, II \tag{14}$$

where

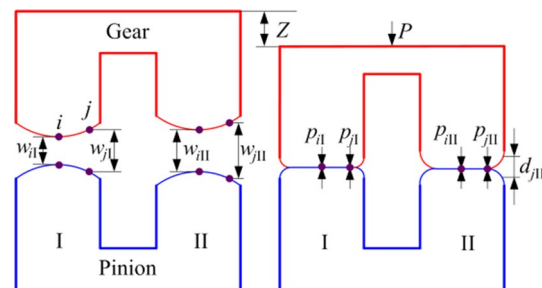


Fig. 5 Model for LTCA of spiral bevel gear

$$w_k = [w_1, w_2, \dots, w_i, w_j, \dots, w_n]^T$$

$$\delta''_k = \delta''[1, 1, \dots, 1, \dots, 1]^T$$

$$b_k = [b_1, b_2, \dots, b_i, b_j, \dots, b_n]^T$$

The parameter δ'' is the gap between two teeth of a meshing gear, and b represents the normal clearance.

If the pinion is fixed and the normal displacement of gear under the load is Z , then the displacement compatibility equation after deformation is as follows:

$$F_k p_k + w_k = Z + d_k \quad k = I, II \tag{15}$$

where

$$p_k = [p_1, p_2, \dots, p_i, p_j, \dots, p_n]^T$$

$$d_k = [d_1, d_2, \dots, d_i, d_j, \dots, d_n]^T$$

$$Z = Z[1, 1, \dots, 1, \dots, 1]^T$$

The parameter p_j ($j = 1, 2, \dots, n$) is the normal load at discrete point j on the major axis of the ellipse, the parameter d_j ($j = 1, 2, \dots, n$) represents the tooth surface clearance at discrete point j on the major axis of the ellipse, and F_k is the comprehensive normal flexibility matrix.

The discrete load p_{jk} satisfies the force equilibrium conditions as follows:

$$\sum_{j=1}^n p_{jI} + \sum_{j=1}^n p_{jII} = P \tag{16}$$

The discrete load p_{jk} and the deformed gap d_{jk} satisfy non embedding conditions as follows:

$$\begin{aligned} p_{jk} > 0 &\Rightarrow d_{jk} = 0 \\ p_{jk} = 0 &\Rightarrow d_{jk} > 0 \end{aligned} \quad (k = I, II) \tag{17}$$

Based on above conditions, a mathematical programming model for the loaded contact problem of spiral bevel gear transmission is established as follows:

$$f = \min \sum_{j=1}^{2n+1} X_j \tag{18}$$

$$w = wFp + Z + d + X$$

$$P = e^T p + X_{2n+1}$$

$$s.t. \quad p_j \geq 0, d_j \geq 0, Z_j \geq 0, X_j \geq 0$$

$$p_j = 0 \quad d_j = 0$$

where X_j ($j = 1, 2, 3, \dots, 2n + 1$) represents an artificial variable. The parameter e is n -dimensional unit column vector.

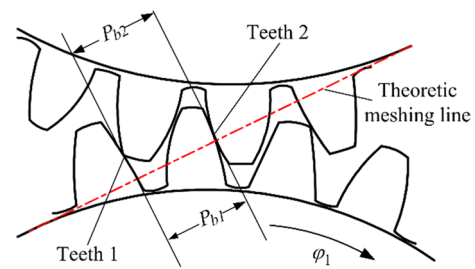


Fig. 6 Meshing impact principle

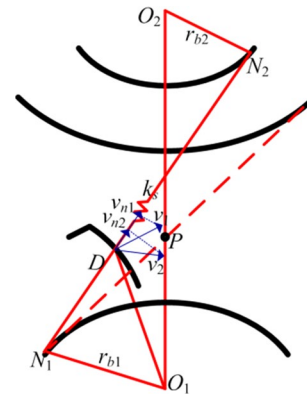


Fig. 7 The impact model

By solving the equations shown above, the normal displacement of the gear under load can be obtained. By converting the normal displacement into angular displacement, the LTE of the gear under a given load can be obtained.

3.2 Meshing Impact

As shown in Fig. 6, during gear transmission, the base pitch difference generated from the loaded deformation results in the speed difference of the gear and pinion at the initial meshing point. The speed difference is the impact velocity. Because of the impact velocity, the impact force will be produced at the initial meshing point. Meshing impact is the main vibration excitation of spiral bevel gear transmission in the high-speed range, and the detailed calculation method of the meshing impact of spiral bevel gear is given in Literature [31].

As shown in Fig. 7, the impact velocity v_s is as follows:

$$v_s = (v_1 - v_2)n_h \tag{19}$$

where v_2 and v_1 is the velocity of the gear and pinion, respectively.

The meshing impact force is as follows:

$$F_s = \left(\frac{n+1}{2} \frac{J_1 J_2}{J_1 r_{b2}^2 + J_2 r_{b1}^2} v_s^2 K_s^{1/n} \right)^{n/(n+1)} \quad (20)$$

where J_1 and J_2 represent the rotary inertia. K_s represents the meshing stiffness. n represents the meshing force exponent coefficient. r_{b1} and r_{b2} represent the instantaneous base circle radius.

3.3 Dynamic analysis

There is vibration excitation in the process of spiral bevel gear transmission, which induces the running vibration of spiral bevel gear transmission. With the development of science, people have put forward higher requirements for the dynamic performance of spiral bevel gear transmission. The traditional dynamic analysis of spiral bevel gears adds the static analysis results into the dynamic equations established by the lumped mass method, and the influence of meshing impact on the dynamic characteristics is not considered, so the calculation results cannot fully conform to the actual situation. Based on TCA and LTCA, the meshing impact of the spiral bevel gear is obtained. According to the dynamic model of the 8-DOF spiral bevel gear shown in Fig. 8, the vibration equation of the spiral bevel gear dynamic model is established as follows. The dynamic response of spiral bevel gear is analyzed by applying LTE excitation and meshing impact excitation in the vibration equation.

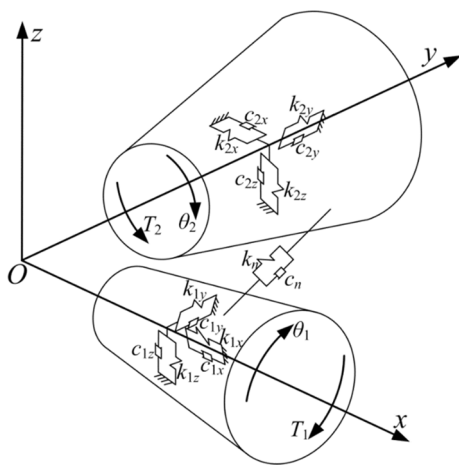


Fig. 8 Dynamic model of 8-DOF spiral bevel gear

$$\begin{cases} m_1 \ddot{X}_1 + c_{1x} \dot{X}_1 + k_{1x} X_1 = -F_x \\ m_1 \ddot{Y}_1 + c_{1y} \dot{Y}_1 + k_{1y} Y_1 = -F_y \\ m_1 \ddot{Z}_1 + c_{1z} \dot{Z}_1 + k_{1z} Z_1 = -F_z \\ J_1 \ddot{\theta}_1 = T_1 - F_n r_1 + F_s r_1 \\ m_2 \ddot{X}_2 + c_{2x} \dot{X}_2 + k_{2x} X_2 = F_x \\ m_2 \ddot{Y}_2 + c_{2y} \dot{Y}_2 + k_{2y} Y_2 = F_y \\ m_2 \ddot{Z}_2 + c_{2z} \dot{Z}_2 + k_{2z} Z_2 = F_z \\ J_2 \ddot{\theta}_2 = -T_2 + F_n r_2 - F_s r_2 \end{cases} \quad (21)$$

where F_s represents the impact force, and it is obtained based on impact theory shown in Sect. 4.2

F_n represents the normal load, $F_n = k_n(t)f(\lambda_n) + c_n \dot{\lambda}_n$

k_n represents the meshing stiffness. LTE (or meshing stiffness) is one of the main vibration excitation of gear transmission.

λ_n represents the normal relative displacement of gear meshing point.

F_x, F_y, F_z represent the components of normal load F_n along $x, y,$ and z axes, respectively.

$d_i (i=1,2,3)$ represents the component of normal vector at meshing point along $x, y,$ and z axes.

k_{1x}, k_{1y} and k_{1z} represent the supporting stiffness of driving gear along $x, y,$ and z axes respectively.

k_{2x}, k_{2y} and k_{2z} represent the supporting stiffness of driven gear along $x, y,$ and z axes respectively.

$k_{1x} = 4.35 \times 10^7$ N/mm. $k_{1y} = 9.4 \times 10^9$ N/mm.

$k_{1z} = 9.4 \times 10^9$ N/mm.

$k_{2x} = 7.3 \times 10^9$ N/mm. $k_{2y} = 1.2 \times 10^8$ N/mm.

$k_{2z} = 7.3 \times 10^9$ N/mm.

m_1 and m_2 represent the mass of driving gear and driven gear respectively.

I_p, I_g represent moment of inertia. $I_p = 0.0024$ kg·m².

$I_g = 0.1527$ kg·m².

m_e represents gear equivalent mass.

$$m_e = \frac{m_1 m_2}{m_1 + m_2} \quad (22)$$

c_n represents meshing damping.

$$c_n = 2\xi \sqrt{k_m m_e} \quad (23)$$

ξ represents the meshing damping ratio, which is 0.08.

c_{1x}, c_{1y} and c_{1z} represent the damping of driving gear along $x, y,$ and z axes respectively.

c_{2x}, c_{2y} and c_{2z} represent the damping of driven gear along $x, y,$ and z axes respectively.

$$c_{ij} = 2\xi \sqrt{k_{ij} m_i} (i = 1, 2, 3; j = x, y, z) \quad (24)$$

Table 1 Geometric parameters

Parameter	Pinion	Gear
Number of teeth	27	74
Module/(mm)	3.85	
Pressure angle/(°)	30	
Mean spiral angle/(°)	30	
Hand of spiral	LH	RH
Shaft angle/(°)	69.77	
Face width/(mm)	38.5	

Table 2 Machine settings based on LSM

Parameter	Gear	Pinion
Radial setting/(mm)	142.3468	155.8422
Initial cradle angle setting/(°)	44.0605	42.3900
Roll ratio	1.2541	3.9013
Vertical offset/(mm)	0	8.0000
Increment of machine centre to back/(mm)	0	22.7800
Sliding base feed setting/(mm)	1.0675	7.2845
Machine root angle/(°)	51.5891	16.3178
Second-order coefficients	0	0.1281
Third-order coefficients	0	0.0167

Table 3 Machine settings based on ease-off technology

Parameter	Gear	Pinion
Radial setting/(mm)	142.3244	134.7376
Initial cradle angle setting/(°)	44.0662	42.7140
Roll ratio	1.2542	3.2680
Vertical offset/(mm)	0	6.4966
Increment of machine centre to back/(mm)	0	2.9737
Sliding base feed setting/(mm)	1.4702	0.3469
Machine root angle/(°)	51.7266	16.1803
Second-order coefficients	0	0.0556
Third-order coefficients	0	0.0708

T_1 and T_2 represent the torque of driving gear and driven gear respectively.

$$T_1 = T_{1m} + T_{1v} \tag{25}$$

$$T_2 = T_{2m} \tag{26}$$

T_{1m} represents average moment, T_{1v} represents variable partial moment, T_{2m} represents constant moment.

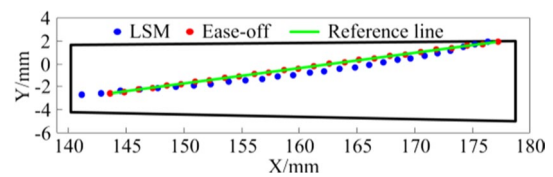


Fig. 9 The contact path of the gear tooth surface

Table 4 Machine settings of pinions based on ease-off technology

Parameter	Pinion 1	Pinion 2
Radial setting/(mm)	139.4247	135.3481
Initial cradle angle setting/(°)	44.4730	43.0967
Roll ratio	3.3613	3.2798
Vertical offset/(mm)	- 0.5889	- 5.6366
Increment of machine centre to back/(mm)	- 2.0390	- 2.9144
Sliding base feed setting/(mm)	0.0865	0.3304
Machine root angle/(°)	16.1803	16.1803
Second-order coefficients	0.0924	0.0331
Third-order coefficients	- 0.0159	0.0231

4 Numerical example

The geometric parameters of the spiral bevel gear are given in Table 1. The machine settings of the spiral bevel gear based on the LSM are given in Table 2. The machine settings of the spiral bevel gear based on ease-off technology are given in Table 3.

The meshing performance of the HCR spiral bevel gear designed by the LSM and ease-off technology is analyzed with the TCA method. The contact path of the gear tooth surface is shown in Fig. 9. By comparison, it is found that the contact path of the HCR spiral bevel gear designed by the LSM is curved, while the contact path of the HCR spiral bevel gear designed based on the ease-off technology is a straight line. Therefore, ease-off technology can overcome the phenomenon that the contact path of the HCR spiral bevel gears designed by the LSM may be seriously bent in the whole meshing process, and then improve the meshing performance and the design level of the HCR spiral bevel gears.

Based on the pre-set geometric TE curve and contact path, the ease-off target surfaces of pinions 1 and 2 are built, respectively. According to the optimization model shown in Eq. 13, the pinion modified tooth surface and the corresponding machining parameters are calculated and listed in Table 4. The meshing performance of the gear pair 1 (composed of pinion 1 and gear) and the gear pair 2 (composed of pinion 2 and gear) is analyzed with the TCA

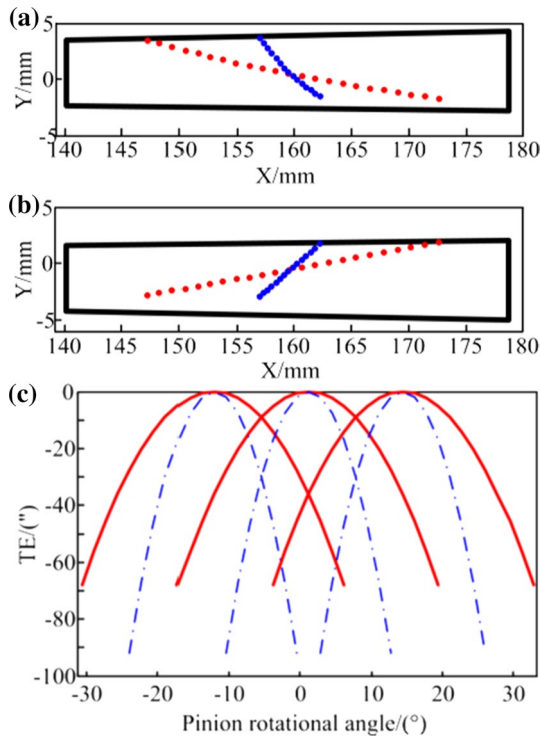


Fig. 10 The TCA results

method. The contact path of the pinion (a) and gear (b) and the transmission error curve (c) are shown in Fig. 10. The blue one is gear pair 1, and the red one is gear pair 2. It is obvious that the angles between the pinion contact path and the pitch cone on the pinion 1 and pinion 2 are 135° and 169° , respectively, and the DCR of gear pair 1 is

1.8, and the DCR of gear pair 2 is 2.8, respectively. Therefore, the DCR of the spiral bevel gear can be improved by increasing the angle between the contact path and the pitch cone on pinion based on ease-off technology.

When the load is 1600 Nm, the LTE of the spiral bevel gear is calculated with the LTCA method, and the calculation results are shown in Fig. 11. By comparison, it is found that the LTE amplitude of gear pair 1 is $4.5270''$ with low-contact-ratio, and the LTE amplitude of gear pair 2 with high-contact-ratio is only $1.6800''$, 62.89% less than gear pair 1 with high-contact-ratio. Therefore, increasing the DCR can reduce the LTE amplitude of the spiral bevel gear. The LTE is one of the main excitations of running vibration and noise of the spiral bevel gear. Therefore, increasing the DCR can improve the dynamic performance of the spiral bevel gear.

To further verify the advantages of the gear pair 2 with high-contact-ratio in reducing LTE, the LTE of the spiral bevel gear obtained by the LTCA method is compared with that obtained by the FEA method. To ensure the accuracy of the FEA results, first, the accuracy of the FEA model should be guaranteed. The accuracy of the FEA model can be divided into the following two parts: tooth surface accuracy and gear assembly accuracy. To ensure the tooth surface accuracy, based on the tooth surface equation, the finite element mesh model of the tooth surface is built by rotating and arraying the position coordinates of discrete points of the tooth surface, and the tooth surface obtained by this method can meet the requirements of high accuracy. The solid model of the gear and the pinion is constructed with discrete points, and the gear and the pinion are placed in the same meshing coordinate system based on the principle of coordinate transformation to complete the assembly of the spiral bevel gear. The seven-tooth FEA model of the spiral bevel gear shown in Fig. 12 is obtained, and the assembly accuracy meets the requirements.

When the load is 1600 Nm, the LTE of the spiral bevel gear is carried out based on the seven-tooth FEA model. In addition, Fig. 11 shows the FEA results. A comparison shows that although the LTE amplitudes obtained by the two

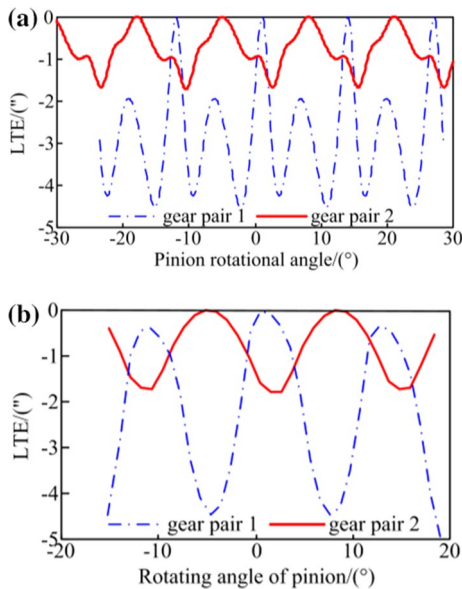


Fig. 11 Comparison of LTE, a LTCA results and b FEA results

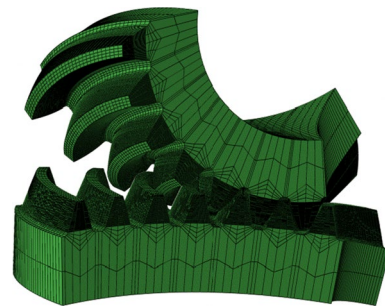


Fig. 12 Finite element analysis model of spiral bevel gear

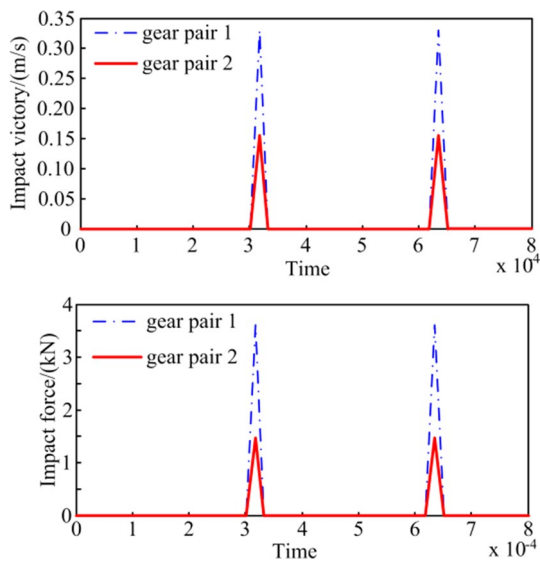


Fig. 13 Comparison of meshing impact

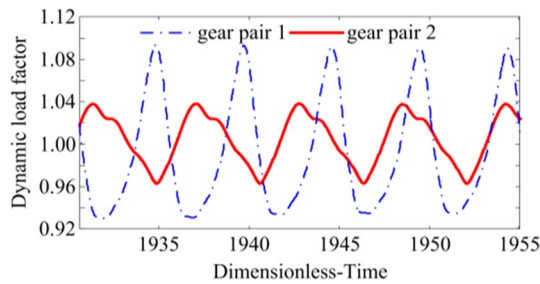


Fig. 14 Comparison of dynamic load factor

methods are slightly different, the variation of the LTE curve is basically the same; gear pair 2 with high-contact-ratio has lower LTE amplitude than gear pair 1 with low-contact-ratio. Therefore, increasing DCR can effectively reduce the LTE of the spiral bevel gear, and improve the meshing performance of the spiral bevel gear.

When the load is 1600 Nm, the pinion rotational speed is 7000 r/min, the meshing impact of the spiral bevel gear is calculated based on the meshing impact theory, and the calculation results are shown in Fig. 13. By comparison, it is found that the impact velocity and impact force of gear pair 1 with low-contact-ratio are 0.3300 m/s and 3610 N, while the impact velocity and impact force of gear pair 2 with high-contact-ratio are 0.1551 m/s and 1466 N, respectively, 53.00% and 59.39% lower than those of gear pair 1 with low-contact-ratio. Therefore, increasing the DCR can reduce the meshing impact of the spiral bevel gear. The meshing impact is one of the main excitations of running vibration and noise of the spiral bevel gear. Therefore, increasing the DCR can improve the dynamic performance of the spiral bevel gear.

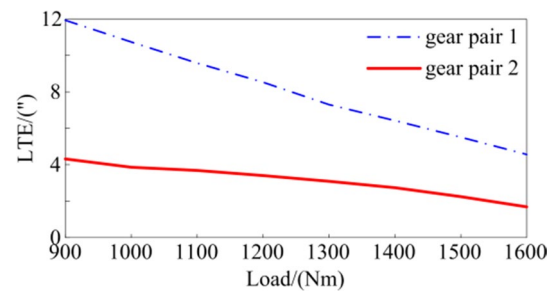


Fig. 15 Comparison of LTE

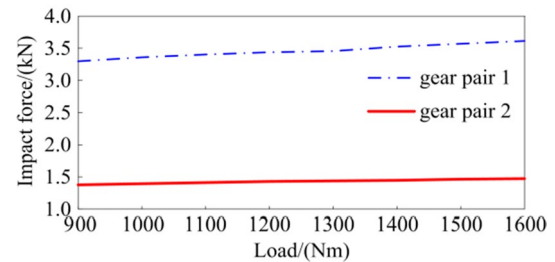
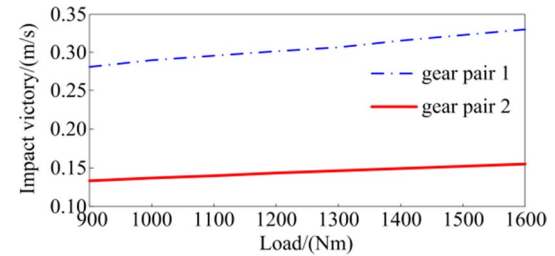


Fig. 16 Comparison of meshing impact

When the load is 1600 Nm, the pinion rotating speed is 7000 r/min. According to the 8-DOF dynamic model established by the lumped mass method as shown in Fig. 8, the dynamic response of the spiral bevel gear is analyzed, and the calculation results are shown in Fig. 14. The dynamic load factor can effectively reflect the vibration characteristics of the spiral bevel gear. The larger the dynamic load factor is, the more severe the vibration is. By comparison, it is found that under the same working conditions, the dynamic load factor of gear pair 1 with low-contact-ratio is 1.0904, while the dynamic load factor of gear pair 2 with high-contact-ratio is only 1.0379. Therefore, increasing the DCR can reduce the dynamic load factor of the spiral bevel gear, and improve the dynamic performance of the spiral bevel gear.

To show the advantage of the HCR spiral bevel gear, the LTEs of gear pair 1 and gear pair 2 under multiple working conditions is analyzed with the LTCA method. The calculation results are shown in Fig. 15. By comparison, it is found that the LTE amplitude of gear pair 1 with low-contact-ratio is larger than gear pair 2 with high-contact-ratio, and they all decrease as the load increases. Therefore, increasing the

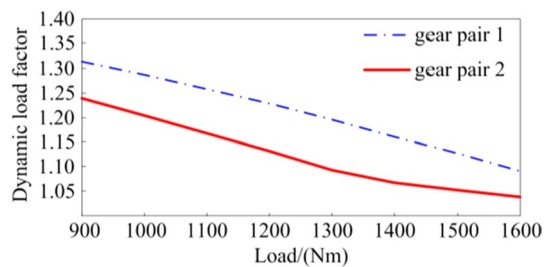


Fig. 17 Comparison of the dynamic load factor

DCR can effectively reduce the LTE amplitude of the spiral bevel gear, and improve the meshing performance of spiral bevel gear transmission.

Then, the meshing impact (the pinion rotational speed is 7000 r/min) of the spiral bevel gear transmission under the multiple working conditions is calculated based on meshing impact theory, and the calculation results are shown in Fig. 16. By comparison, it is found that the impact velocity and impact force of gear 2 with high-contact-ratio are both smaller than those of gear pair 1 with low-contact-ratio. Furthermore, the impact velocity and impact force both increase with increasing loads. Therefore, increasing the DCR can effectively reduce the meshing impact of the spiral bevel gear and improve the meshing performance of the spiral bevel gear.

When the rotating speed is 7000 r/min, the dynamic response of the spiral bevel gear is analyzed based on the 8-DOF dynamic model shown in Fig. 8, and the calculation results are shown in Fig. 17. By comparison, it is found that under the same working conditions, the dynamic load factors of gear pair 2 with high-contact-ratio are smaller than those of gear pair 1 with low-contact-ratio. Therefore, increasing the DCR can effectively reduce the dynamic load factor, and improve the dynamic performance of the spiral bevel gear.

5 Conclusions

The LTE (the main vibration excitation of gear transmission in the low-speed range) and meshing impact (the main vibration excitation of gear transmission in the high-speed range) are the main vibration excitations of aviation spiral bevel gear. To improve the dynamic performance of the spiral bevel gear, an ease-off flank modification method for the HCR spiral bevel gear is proposed by increasing the angle between the contact path and the pitch cone on the pinion tooth surface. According to the simulation analysis of the HCR spiral bevel gear designed based on ease-off technology, the following results are obtained:

- (1) The contact path of the HCR spiral bevel gear designed by the LSM is curved, while the contact path of the HCR spiral bevel gear designed based on ease-off technology is a straight line. Therefore, ease-off technology can effectively improve the meshing performance of the HCR spiral bevel gear.
- (2) Under the same working conditions, the LTE, meshing impact, and dynamic load factor of the HCR spiral bevel gear are all smaller than those of the low-contact-ratio spiral bevel gear. Therefore increasing the DCR can effectively reduce the dynamic load factor of the spiral bevel gear, and improve the dynamic performance of the spiral bevel gear.
- (3) Aimed at the variable working conditions of the spiral bevel gear, the LTE, meshing impact and dynamic load factor of the HCR spiral bevel gear under multiple loads are analyzed. It is found that increasing the DCR can effectively improve the dynamic performance of the spiral bevel gear.

The HCR design method based on ease-off technology can be used for the design and analysis of other gear pairs.

Acknowledgements We thank the support from the Fundamental Research Funds for the Central Universities (No. JUSRP12059), the Jiangsu Key Laboratory of Advanced Food Manufacturing Equipment and Technology (No. FMZ202021), the National Science Foundation of China (No. 51975251), the Natural Science Foundation of Jiangsu Province (No. BK20160181). We also thank all reviewers and editors for their valuable comments and suggestions.

References

1. Falah, B., Gosselin, C., & Cloutier, L. (1998). Experimental and numerical investigation of the meshing cycle and contact ratio in spiral bevel gears. *Mechanism and Machine Theory*, 33(1–2), 21–37.
2. Kahraman, A., & Blankenship, G. W. (1999). Effect of involute contact ratio on spur gear dynamics. *ASME Journal of Mechanical Design*, 121(1), 112–118.
3. Deng, X. Z., Fan, M., & Yang, H. B. (2002). Relationship between contact ratio and load of spiral bevel gears. *China Mechanical Engineering*, 12(8), 878–880. Chinese.
4. Deng, X. Z., Fang, Z. D., & Zhang, J. L. (2002). Design of spiral bevel gears with high contact ratio. *China Mechanical Engineering*, 13(9), 791–795. Chinese.
5. Deng, X. Z., Fang, Z. D., & Yang, H. B. (2002). Strength analysis of spiral bevel gear with high contact ratio. *Journal of Aerospace Power*, 17(3), 367–372. Chinese.
6. Deng, X. Z. (2002). *Research of design theory and experiments of spiral bevel gears with high contact ratio*. Northwestern Polytechnical University. Chinese.
7. Deng, X. Z., Fang, Z. D., & Wei, B. Y. (2004). Design and experiment of spiral bevel gears with high contact ratio. *Chinese Journal of mechanical Engineering*, 40(6), 95–99. Chinese.
8. Wildhaber, E. (1946). Basic relationship of hypoid gears. *American Machinist*, 90(6), 108–111.

9. Baxter, L. M. (1961). Basic geometry and tooth contact of hypoid gears. *Industrial Mathematics*, 11, 1–28.
10. Litvin, F. L., & Cutman, Y. (1981). A method of local synthesis of gears grounded on the connection between the principal and geodetic curvatures of surfaces. *ASME Journal of Mechanical Design*, 103, 114–125.
11. Litvin, F. L., & Zhang, Y. (1991). *Local synthesis and tooth contact analysis of face-milled spiral bevel gears*. NASA Lewis Research Center.
12. Shih, Y. P., & Fong, Z. H. (2007). Flank modification methodology for face-hobbing hypoid gears based on ease-off topography. *ASME Journal of Mechanical Design*, 12(129), 1294–1302.
13. Shih, Y. P. (2010). A novel ease-off flank modification methodology for spiral bevel and hypoid gears. *Mechanism and Machine Theory*, 45(8), 1108–1124.
14. Shih, Y. P. (2007). *Study on the flank modification of face hobbed hypoid gears*. National Chung Cheng University.
15. Standfield, H. J. (2000). The ultimate motion graph. *ASME Journal of Mechanical Design*, 9(122), 316–322.
16. Kolivand, M., & Kahraman, A. (2009). A load distribution model for hypoid gears using ease-off topography and shell theory. *Mechanism and Machine Theory*, 10(44), 1848–1865.
17. Kolivand, M., & Kahraman, A. (1946). An ease-off based method for loaded tooth contact analysis of hypoid gears having local and global surface deviations. *ASME Journal of Mechanical Design*, 132(7), 071004.
18. Artoni, A., Kolivand, M., & Kahraman, A. (2010). An ease-off based optimization of the loaded transmission error of hypoid gears. *ASME Journal of Mechanical Design*, 1(132), 011010.
19. Artoni, A., Gabivvini, M., & Kolivand, M. (2013). Ease-off based compensation of tooth surface deviations for spiral bevel and hypoid gears: Only the pinion needs corrections. *Mechanism and Machine Theory*, 1(61), 84–101.
20. Fan, Q. (2016). *Ease-off and application in tooth contact analysis for face-milled and face-hobbed spiral bevel and hypoid gears*. Springer International Publishing.
21. Wang, Q., Zhou, C., & Gui, L. J. (2018). Optimization of the loaded contact pattern of spiral bevel and hypoid gears based on a kriging model. *Mechanism and Machine Theory*, 122, 432–449.
22. Ding, H., Tang, J. Y., & Zhong, J. (2016). An accurate model of high-performance manufacturing spiral bevel and hypoid gears based on machine setting modification. *Journal of Manufacturing Systems*, 41, 111–119.
23. Ding, H., Tang, J. Y., & Zhou, Y. S. (2017). A multi-objective correction of machine settings considering loaded tooth contact performance in spiral bevel gears by nonlinear interval number optimization. *Mechanism and Machine Theory*, 113, 85–108.
24. Ding, H., Wan, G., & Zhou, Y. S. (2017). Nonlinearity analysis based algorithm for indentifying machine settings in the tooth flank topography correction for hypoid gears. *Mechanism and Machine Theory*, 113, 1–21.
25. Rong, K. B., Ding, H., & Tang, J. Y. (2020). Adaptive data-driven modular control approach to computer aided process planning for manufacturing spiral bevel and hypoid gears. *Proceedings of the Institution of Mechanical Engineers, Part B: Journal of Engineering Manufacture*, 235(2), 0954405420956767.
26. Mu, Y. M., & Fang, Z. D. (2017). Design and analysis of high contact ratio spiral bevel gears by modified curvature motion method. *Proceedings of the Institution of Mechanical Engineers Part C-Journal of Mechanical Engineering Science*, 232, 3396–3409.
27. Mu, Y. M. (2017). An ease-off flank modification method for high contact ratio spiral bevel gears with modified curvature motion. *Journal of Advanced Mechanical Design Systems and Manufacturing*, 11, JAMDSM00344.
28. Mu, Y. M., He, X. M., & Fang, Z. D. (2021). An innovative ease-off flank modification method based on the dynamic performance for high-speed spiral bevel gear with high-contact-ratio. *Mechanism and Machine Theory*, 162, 104345.
29. Mu, Y. M., & He, X. M. (2021). Design and dynamic performance analysis of high-contact-ratio spiral bevel gear based on the higher-order tooth surface modification. *Mechanism and Machine Theory*, 161, 104312.
30. Simon, V. (2009). Loaded tooth contact analysis and stresses in spiral bevel gear. In: Proceedings of ASME design engineering technical conference.
31. Mu, Y. M., & Fang, Z. D. (2019). Impact analysis and vibration reduction design of spiral bevel gears. *Proceedings of the Institution of Mechanical Engineers, Part K: Journal of Multi-body Dynamics*, 23, 668–676.

Publisher's Note Springer Nature remains neutral with regard to jurisdictional claims in published maps and institutional affiliations.



Yan-Ming Mu was born in Yantai, Shandong, China in 1987. He received the Ph.D. degree from the School of Mechanical Engineering, Northwestern Polytechnical University, Xi'an, China, in 2019. He worked in School of Mechanical Engineering, Jiangnan University, Wuxi. His current research interests include the design and inspection of tooth surface of spiral bevel gear and dynamic analysis of spiral bevel gear.



Xue-Ming He was born in Suzhou, China in 1966. He received the Ph.D. degree from the School of Mechanical Science and Engineering, Huazhong University of Science and Technology, Wuhan, China, in 2011. He worked in the School of Mechanical Engineering, Jiangnan University, Wuxi. His current research interests include digital design and dynamic thermal fluid.



Zong-De Fang was born in Shanghai, China in 1948. He received the Ph.D. degree from the Department of Automotive Engineering, Tsinghua University, Beijing, China, in 1986. He worked in the School of Mechanical Engineering, Northwestern Polytechnical University, Xi'an. His current research interests include gear meshing theory, tooth surface design.